Journal of Sound and Vibration (1998) **212**(4), 721–742

VIBRATION SUPPRESSION AND MOTION CONTROL OF A NON-LINEARLY COUPLED FLEXIBLE QUICK-RETURN MECHANISM DRIVEN BY A PM SYNCHRONOUS SERVO MOTOR

RONG-FONG FUNG AND KEN-WANG CHEN

Department of Mechanical Engineering, Chung Yuan Christian University, Chung-Li, Taiwan 32023, *R.O.C.*

(*Received* 3 *July* 1997, *and in final form* 16 *December* 1997)

This paper studies both speed and tracking controls of a non-linear flexible quick-return mechanism driven by a permanent magnet (PM) synchronous servo motor. A flexible rod of the mechanism is divided into two regions. Each region has a time-dependent length and is modelled by the Timoshenko beam theory. The finite element method (FEM) with time-dependent length and Hamilton's principle are utilized to derive the governing equation. Variable structure control (VSC) is applied to reduce the flexible vibrations. In order to control the crank motion and suppress the motion-induced vibrations simultaneously, both speed and tracking controllers are designed by the reaching law variable structure control method. Simulation results show that the dynamic behaviour of the proposed controller–motor–mechanism system is performed to eliminate the tip deflections of the flexible rod and have a good performance. Moreover, the robustness against the external disturbances is also improved by employing the proposed control scheme.

1. INTRODUCTION

The traditional approach to dynamic analysis of mechanism and machines is based on the assumption that systems are composed of rigid bodies. However, when a mechanism operates in a high-speed condition, the rigid-body assumption is no longer valid and the links should be considered flexible. Whitworth quick-return mechanism had been modified and used for constructing a high-speed impacting press. Dwivedi [1] presented an approximate expression for the angular displacement, velocity and acceleration of the mechanism. The quick-return mechanism was investigated by Beale and Scott [2, 3] on the deflection and stability whereas the rod was considered as an Euler–Bernoulli Beam. Spatial dependence was eliminated by using Galerkin's method with time-dependent pinned-pinned overhanging beam modes. Moreover, Lee [4] presented the dynamics of a flexible rod in a quick-return mechanism. However, Galerkin's approach is too computationally intensive due to the time-dependent boundary and its complex mode shape.

Most works on the dynamics and stability of a flexible rod of a quick-return mechanism are based on the finite element method (FEM). For examples, Bahgat and Willmert [5], Song and Haug [6] and Yang and Sadler [7] employed FEM in their works to investigate the dynamics of the flexible planar mechanisms. Fung and Lee [8] obtained the stability of a quick-return mechanism with time-dependent coefficients by FEM. The flexible

0022–460X/98/190721 + 22 $25.00/0/sv971470

multibody machine tool mechanism subjected to constant and chattering cutting forces was analysed by Shabana and Thomas [9]. Generally speaking, the previous studies described the motion of the flexible rod by using the Euler beam theory. Heretofore, little work is emphasized on both speed control and vibration suppression of the quick-return mechanisms.

The earliest studies in control of a two-link flexible manipulator were presented by Book *et al*. [10]. In order to assure system robustness, Flcola *et al*. [11] presented a simplified strategy to implement sliding mode control of a two-joints robot with a flexible forearm. A sliding mode control scheme was developed by Yeung and Chen [12, 13] for the regulation of a one-link flexible arm. Choi *et al*. [14] formulated a new sliding mode controller for the tip position control of a single-link flexible manipulator subjected to parameter variations. In the previous works, the utilization of the sliding mode control is limited in the area of the flexible manipulators.

In recent years, advancements in magnetic materials, semiconductor power devices, and control theory have made the permanent magnet (PM) synchronous servo motors drive play a vitally important role in motion-control applications in the low-to-medium power range. The desirable features of the PM synchronous servo motors are its compact structure, high air-gap flux density, high power density, high torque-to-inertia ratio, and high torque capability. Moreover, compared with the induction servo motors, the PM synchronous servo motors have such advantages as higher efficiency, due to the absence of rotor losses and lower no-load current below the rated speed; and its decoupling control performance is much less sensitive to the parametric variation of the motor [15, 16]. To achieve fast four-quadrant operation and smooth starting and acceleration, the field-oriented control [17], or vector control, is used in the design of the PM synchronous servo motor drive.

In this study, the main objective is focused on both speed and tracking controls of a PM synchronous servo motor coupled with a flexible quick-return mechanism. First, the coordinate partitioning method of kinematic analysis is used to deal with the constraint condition of the mechanism. Next, in order to control the coupled motor-mechanical system with robust characteristics, variable structure controllers are designed to control the crank rotating with a constant angular velocity and the desired trajectories. Then, a nonlinear flexible quick-return mechanism system actuated by a PM synchronous servo motor drive is formulated by the FEM. Numerical results show that the dynamic behavior of the controller-motor-mechanism system not only reduces the dynamic deflections of the flexible connecting rod, but also keeps good performances. It also shows that the proposed variable structure control (VSC) is robust with respect to the external disturbances.

2. COORDINATE PARTITIONING METHOD OF KINEMATIC ANALYSIS

In kinematic analysis, the constraint equations occur often in the mechanism. It is required that the coordinate partitioning method be used [18] to partition the coordinate vector as

$$\mathbf{Q} = [\mathbf{Q}_1, \mathbf{Q}_2, \ldots, \mathbf{Q}_n]^T = [\mathbf{p}^T, \mathbf{q}^T]^T,$$

where $\mathbf{p} = [p_1, p_2, \ldots, p_m]^T$ and $\mathbf{q} = [q_1, q_2, \ldots, q_k]^T$ are the m dependent and k independent coordinates respectively. The m constraint equations

$$\mathbf{\Phi} \equiv \mathbf{\Phi}(\boldsymbol{Q}) = \mathbf{0}, \tag{1}$$

must be expressed as

$$\boldsymbol{\Phi} \equiv \boldsymbol{\Phi}(\boldsymbol{p}, \boldsymbol{q}) = \mathbf{0}. \tag{2}$$

Constraint equations as represented by (2) are usually nonlinear. For position analysis, iteration of numerical method may be used to solve the set of nonlinear algebraic equations. Since the k independent coordinates are specified at each instant of time t, (2) becomes a set of m equations in m unknowns and can be solved for the m dependent coordinates. If the constraints of (1) are independent, the existence of a solution $\boldsymbol{p}$ for a given $\boldsymbol{q}$ is asserted by the implicit function theory.

Differentiating (1) yields the constraint velocity equation

$$\boldsymbol{\Phi}_Q \dot{\boldsymbol{Q}} = \mathbf{0}, \tag{3}$$

where matrix $\boldsymbol{\Phi}_Q = [\partial \boldsymbol{\Phi}/\partial \boldsymbol{Q}]$ is the partial derivative of the constraint equations with respect to the coordinate and is called the constraint Jacobian matrix. Sequentially, (3) is rewritten in partitioned form as

$$\boldsymbol{\Phi}_p \dot{\boldsymbol{p}} = -\boldsymbol{\Phi}_q \dot{\boldsymbol{q}}, \tag{4}$$

where $\boldsymbol{\Phi}_p$ and $\boldsymbol{\Phi}_q$ are two submatrices of $\boldsymbol{\Phi}_Q$. Since the m constraint equations (1) are assumed to be independent, then $\boldsymbol{\Phi}_p$ is a $m \times m$ nonsingular matrix. Sequentially, (4) may be solved directly for $\dot{\boldsymbol{p}}$, once $\dot{\boldsymbol{q}}$ is given.

Differentiating the constraint velocity equation (3), we obtain the acceleration equation

$$\boldsymbol{\Phi}_Q \ddot{\boldsymbol{Q}} = -(\boldsymbol{\Phi}_Q \dot{\boldsymbol{Q}})_Q \dot{\boldsymbol{Q}} \equiv \boldsymbol{\gamma}, \tag{5}$$

where $\ddot{\mathbf{Q}} = [\ddot{Q}_1, \ddot{Q}_2, \ldots, \ddot{Q}_n]^T$ is the acceleration vector. In the mean time, (5) can be written in partitioned form as

$$\boldsymbol{\Phi}_p \ddot{\boldsymbol{p}} = -\boldsymbol{\Phi}_q \ddot{\boldsymbol{q}} - (\boldsymbol{\Phi}_Q \dot{\boldsymbol{Q}})_Q \dot{\boldsymbol{Q}}. \tag{6}$$

Since $\boldsymbol{\Phi}_p$ is nonsingular, (6) can be solved for $\ddot{\boldsymbol{p}}$, once $\ddot{\boldsymbol{q}}$ is given. Note that the velocity (4) and acceleration (6) are two sets of linear algebraic equations in $\dot{\boldsymbol{Q}}$ and $\ddot{\boldsymbol{Q}}$ respectively.

In general situation, the Euler–Lagrange equation [18] accounting for both applied and constraint forces is

$$\boldsymbol{M}(\boldsymbol{Q})\ddot{\boldsymbol{Q}} + \boldsymbol{N}(\boldsymbol{Q}, \dot{\boldsymbol{Q}}) + \boldsymbol{\Phi}_Q^T \boldsymbol{\Lambda} = \boldsymbol{B}\boldsymbol{U}, \tag{7}$$

where $\boldsymbol{M}$ is a mass matrix, $\boldsymbol{N}$ is a nonlinear vector, $\boldsymbol{\Lambda}$ is the Lagrange multiplier, $\boldsymbol{B}$ is a constant matrix and $\boldsymbol{U}$ is a vector of applied forces.

In addition to equation (7), the acceleration equation (5) must hold. We combine (7) and (5) in matrix form as

$$\begin{bmatrix} \boldsymbol{M} & \boldsymbol{\Phi}_Q^T \\ \boldsymbol{\Phi}_Q & \mathbf{0} \end{bmatrix} \begin{bmatrix} \ddot{\boldsymbol{Q}} \\ \boldsymbol{\Lambda} \end{bmatrix} = \begin{bmatrix} \boldsymbol{B}\boldsymbol{U} - \boldsymbol{N}(\boldsymbol{Q}, \dot{\boldsymbol{Q}}) \\ \gamma \end{bmatrix}. \tag{8}$$

This is a system of differential-algebraic equation.

The differential-algebraic equation of mechanism motion derived above is summarized in the matrix form (8). Implicit method will be employed to solve the equation (8) by reordering and partitioning. According to the decomposition of $\boldsymbol{Q}$ into $\boldsymbol{p}$ and $\boldsymbol{q}$, we have

$$\begin{aligned} \boldsymbol{M}^{pp}\ddot{\boldsymbol{p}} + \boldsymbol{M}^{pq}\ddot{\boldsymbol{q}} + \boldsymbol{\Phi}_p^T \boldsymbol{\Lambda} &= \boldsymbol{B}^p \boldsymbol{U} - \boldsymbol{N}^p, \\ \boldsymbol{M}^{qp}\ddot{\boldsymbol{p}} + \boldsymbol{M}^{qq}\ddot{\boldsymbol{q}} + \boldsymbol{\Phi}_q^T \boldsymbol{\Lambda} &= \boldsymbol{B}^q \boldsymbol{U} - \boldsymbol{N}^q, \\ \boldsymbol{\Phi}_p \ddot{\boldsymbol{p}} + \boldsymbol{\Phi}_q \ddot{\boldsymbol{q}} &= \boldsymbol{\gamma}. \end{aligned} \tag{9}$$

In the above equations, eliminating $\boldsymbol{\Lambda}$ and $\ddot{\boldsymbol{p}}$ yields

$$\hat{\boldsymbol{M}}(\boldsymbol{q})\ddot{\boldsymbol{q}} + \hat{\boldsymbol{N}}(\boldsymbol{q}, \dot{\boldsymbol{q}}) = \hat{\boldsymbol{Q}}\boldsymbol{U}, \tag{10}$$

where

$$\hat{\boldsymbol{M}} = \boldsymbol{M}^{qq} - \boldsymbol{M}^{qp}\boldsymbol{\Phi}_p^{-1}\boldsymbol{\Phi}_q - \boldsymbol{\Phi}_q^T(\boldsymbol{\Phi}_p^{-1})^T[\boldsymbol{M}^{pq} - \boldsymbol{M}^{pp}\boldsymbol{\Phi}_p^{-1}\boldsymbol{\Phi}_q],$$

$$\hat{\boldsymbol{N}} = [\boldsymbol{N}^q - \boldsymbol{\Phi}_q^T(\boldsymbol{\Phi}_p^{-1})^T\boldsymbol{N}^p] + [\boldsymbol{M}^{qp}\boldsymbol{\Phi}_p^{-1} - \boldsymbol{\Phi}_q^T(\boldsymbol{\Phi}_p^{-1})^T\boldsymbol{M}^{pp}\boldsymbol{\Phi}_p^{-1}]\boldsymbol{\gamma},$$

$$\hat{\boldsymbol{Q}} = \boldsymbol{B}^q - \boldsymbol{\Phi}_q^T(\boldsymbol{\Phi}_p^{-1})^T\boldsymbol{B}^p.$$

Equation (10) is a set of differential equations in terms of the independent coordinate $\boldsymbol{q}$ only and is an initial value problem.

Let $\boldsymbol{X} = [\boldsymbol{q}^T \ \dot{\boldsymbol{q}}^T]^T$ be the state variable vector. One can rewrite (10) in terms of $\boldsymbol{X}$ as

$$\dot{\boldsymbol{X}} = \hat{\boldsymbol{a}}(\boldsymbol{X}) + \hat{\boldsymbol{b}}\boldsymbol{U}, \tag{11}$$

where

$$\hat{\boldsymbol{a}}(\boldsymbol{X}) = \begin{bmatrix} \dot{\boldsymbol{q}} \\ -\hat{\boldsymbol{M}}^{-1}\hat{\boldsymbol{N}} \end{bmatrix}, \qquad \hat{\boldsymbol{b}} = \begin{bmatrix} \boldsymbol{0} \\ \hat{\boldsymbol{M}}^{-1}\hat{\boldsymbol{Q}} \end{bmatrix}.$$

3. DESIGN OF VARIABLE STRUCTURE CONTROLLER

Variable structure system (VSS) is a special class of nonlinear systems characterized by a discontinuous control action which changes the system structure on the switching surface. The major merit of VSS is its insensitivity to parameter variations and external disturbances. In this section, the first subject is to design the switching functions, and the next one is to design the reaching mode and the overall control law. The main requirement in the design is that the control should satisfy the reaching condition, which guarantees the existence of a sliding mode on the switching surface.

3.1. SWITCHING SURFACE SCHEME

In switching surface design, it is essential to use error signal and its derivatives to form the coordinates and switching surface. When the state variable slides on the switching surface and to the origin, the system error goes to zero and the desired target state is reached.

In this study, the quick-return mechanism is one degree-of-freedom, and only one input is needed for the motor-mechanism coupled system. Rewriting (10) as

$$\ddot{\boldsymbol{q}} = \boldsymbol{a}(\boldsymbol{q}, \dot{\boldsymbol{q}}) + \boldsymbol{b}(\boldsymbol{q})\boldsymbol{U}, \tag{12}$$

where $\boldsymbol{a}(\boldsymbol{q}, \dot{\boldsymbol{q}}) = -\hat{\boldsymbol{M}}^{-1}\hat{\boldsymbol{N}}$, $\boldsymbol{b}(\boldsymbol{q}) = \hat{\boldsymbol{M}}^{-1}\hat{\boldsymbol{Q}}$ and $\boldsymbol{U}$ is the control input.

Speed and trajectory controllers [19–21] using the VSC reaching mode method are proposed for various systems. To control the speed $\dot{\boldsymbol{q}}$, many more sophisticated schemes will be necessary. Unlike the conventional VSC, the integral variable structure control (IVSC) applied in the speed control is suitable for the system without any information of acceleration.

3.1.1. *Speed controller design*

Let the speed error vector be

$$\boldsymbol{e} = \dot{\boldsymbol{q}} - \dot{\boldsymbol{q}}_d, \tag{13}$$

where the speed desired vector $\dot{\boldsymbol{q}}_d$ is constant. The resultant error state equation is

$$\dot{\boldsymbol{e}} = \ddot{\boldsymbol{q}} - \ddot{\boldsymbol{q}}_d = \boldsymbol{a}(\boldsymbol{q}, \dot{\boldsymbol{q}}) + \boldsymbol{b}(\boldsymbol{q})\boldsymbol{U} - \ddot{\boldsymbol{q}}_d. \tag{14}$$

Only one control input is needed in the motor-mechanism coupled system; a single switching surface $S(\boldsymbol{e})$ will be constructed for the system. By using a scalar function with the integration of the speed error vector $\boldsymbol{e}$, we have the switching function [21]

$$S(\boldsymbol{e}) = \boldsymbol{C}_1\boldsymbol{e} + \boldsymbol{C}_2 \int_0^t \boldsymbol{e}(\eta)\, \mathrm{d}\eta. \tag{15}$$

It is noted that (15) is an IVSC. In the conventional VSC, it produces the undesirable steady-state error owing to the nonideal sliding mode. The proposed IVSC scheme for speed control gives the additional advantage of improving the steady-state performance.

Substituting (14) into the time derivative of $S(\boldsymbol{e})$, one obtains

$$\dot{\boldsymbol{S}} = \boldsymbol{C}_1\dot{\boldsymbol{e}} + \boldsymbol{C}_2\boldsymbol{e} = \boldsymbol{C}_1[\boldsymbol{a}(\boldsymbol{q}, \dot{\boldsymbol{q}}) + \boldsymbol{b}(\boldsymbol{q})\boldsymbol{U} - \ddot{\boldsymbol{q}}_d] + \boldsymbol{C}_2\boldsymbol{e}. \tag{16}$$

Figure 1 shows the block diagram of the constant speed controller applied to a flexible mechanism driven by a PM synchronous servo motor.

3.1.2. *Tracking controller design*

The tracking error vector of the system is

$$\tilde{\boldsymbol{e}} = \boldsymbol{X} - \boldsymbol{X}_d = \begin{bmatrix} \tilde{\boldsymbol{e}}_i \\ \dot{\tilde{\boldsymbol{e}}}_i \end{bmatrix} = \begin{bmatrix} \boldsymbol{q} - \boldsymbol{q}_d \\ \dot{\boldsymbol{q}} - \dot{\boldsymbol{q}}_d \end{bmatrix}, \tag{17}$$

where $\boldsymbol{X}_d = [\boldsymbol{q}_d^T \;\; \dot{\boldsymbol{q}}_d^T]^T$. The first and second derivatives of $\tilde{\boldsymbol{e}}_i$ are defined as the following

$$\dot{\tilde{\mathbf{e}}}_\mathbf{i} = \tilde{\mathbf{e}}_\mathbf{j} = \dot{\mathbf{q}} - \dot{\mathbf{q}}_\mathbf{d}, \tag{18a}$$

$$\dot{\tilde{\mathbf{e}}}_\mathbf{j} = \ddot{\mathbf{q}} - \ddot{\mathbf{q}}_\mathbf{d} = \mathbf{a}(\mathbf{q}, \dot{\mathbf{q}}) + \mathbf{b}(\mathbf{q})\mathbf{U} - \ddot{\mathbf{q}}_\mathbf{d}. \tag{18b}$$

A single switching function $S(\tilde{\boldsymbol{e}})$ for the system (18a, b) is

$$\mathbf{S}(\tilde{\mathbf{e}}) = \mathbf{C}\tilde{\mathbf{e}} = [\mathbf{C}_\mathbf{i} \quad \mathbf{C}_\mathbf{j}]\begin{bmatrix} \tilde{\mathbf{e}}_\mathbf{i} \\ \tilde{\mathbf{e}}_\mathbf{j} \end{bmatrix} = \mathbf{C}_\mathbf{i}\tilde{\mathbf{e}}_\mathbf{i} + \mathbf{C}_\mathbf{j}\tilde{\mathbf{e}}_\mathbf{j}, \tag{19}$$

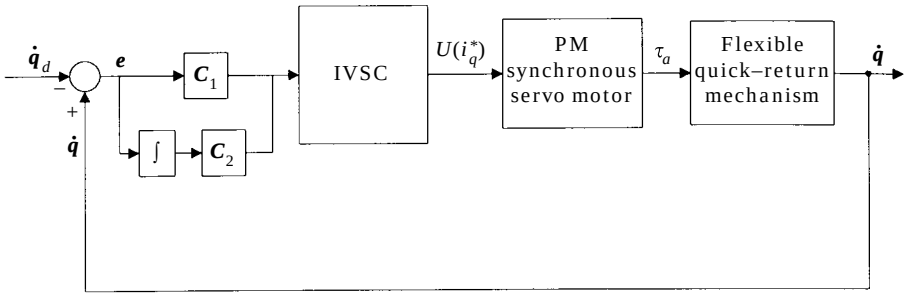

Figure 1. Block diagram of a constant speed controller applied to a flexible quick-return mechanism driven by a PM synchronous servo motor with IVSC.

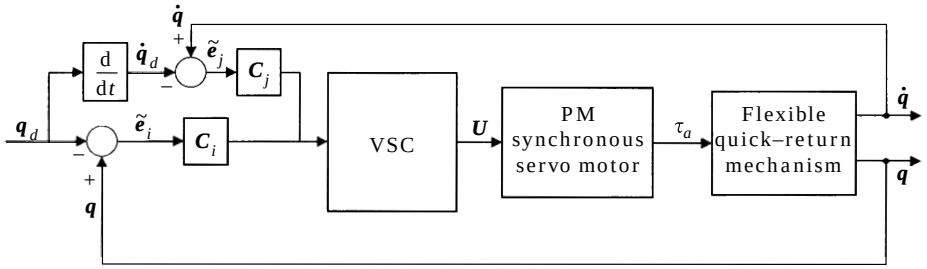

Figure 2. Block diagram of a tracking controller applied to a flexible quick-return mechanism driven by a PM synchronous servo motor with VSC.

Substituting (18a, b) into the time derivative of $S(\tilde{\boldsymbol{e}})$, one can obtain

$$\dot{\mathbf{S}} = \mathbf{C}_i\dot{\tilde{\mathbf{e}}}_i + \mathbf{C}_j\dot{\tilde{\mathbf{e}}}_j = \mathbf{C}_i\tilde{\mathbf{e}}_j + \mathbf{C}_j[\mathbf{a}(\mathbf{q}, \dot{\mathbf{q}}) + \mathbf{b}(\mathbf{q})\mathbf{U} - \ddot{\mathbf{q}}_d]. \tag{20}$$

The position control can also be given by the tracking control as if the desired position, speed and acceleration are time-independent. Figure 2 shows the block diagram of the tracking controller.

3.2. REACHING MODE DESIGN AND CONTROL LAW

The treatment given here is to define the reaching law with proportional plus constant power rates:

$$\dot{S} = -PS - Q|S|^k \operatorname{sgn}(S), \qquad 0 < \kappa < 1, \tag{21}$$

where P and Q are positive constant coefficients. This reaching law will decrease the reaching time when the state is far away from the switching surface [22, 23]. Thus, by choice of the above reaching law (21), states are forced to approach the switching surface faster and the chattering is also suppressed. It is noted that the selection of (21) guarantees the convergence of the trajectories to the switching surface. Sliding will occur along the hyperplane $S = 0$ as long as the necessary hitting condition [24]:

$$S\dot{S} < 0. \tag{22}$$

By substituting (15) and (16) into (22) for the speed controller and substituting (19) and (20) into (22) for the tracking controller, the hitting condition (22) is always satisfied regardless of the signs in (15) and (19). Thus, we can obtain the control laws as follows.

3.2.1. *Speed controller design*

The control input for the speed controller design is

$$\boldsymbol{U} = -(\boldsymbol{C}_1\boldsymbol{b}(\boldsymbol{q}))^{-1}[\boldsymbol{C}_2\boldsymbol{e} + \boldsymbol{C}_1(\boldsymbol{a}(\boldsymbol{q}, \dot{\boldsymbol{q}}) - \ddot{\boldsymbol{q}}_d) + PS + Q|S|^k \operatorname{sgn}(S)]. \tag{23}$$

3.2.2. *Tracking controller design*

The control input for the tracking controller design is

$$\boldsymbol{U} = -(\boldsymbol{C}_j\boldsymbol{b}(\boldsymbol{q}))^{-1}[\boldsymbol{C}_i\tilde{\boldsymbol{e}}_j + \boldsymbol{C}_j(\boldsymbol{a}(\boldsymbol{q}, \dot{\boldsymbol{q}}) - \ddot{\boldsymbol{q}}_d) + PS + Q|S|^k - \operatorname{sgn}(S)]. \tag{24}$$

In order to reduce the chattering, we approximate the sgn (S) in the discontinuous control laws (23) and (24) by a saturation function inside the boundary layer [19]. The saturation function is

$$\text{sat}(S) = \begin{cases} S/\Delta, & |S| \leqslant \Delta \\ \text{sgn}(S), & |S| > \Delta \end{cases}, \tag{25}$$

where Δ is a boundary layer width.

4. FLEXIBLE QUICK-RETURN MECHANISM

The matrix form of motion equation for a flexible quick-return mechanism will be derived by using Hamilton's principle and FEM. The control input applied to the crank is supplied by a PM synchronous servo motor.

4.1. SYSTEM DESCRIPTION

The undeformed configuration of the flexible slider-crank mechanism driven by a PM synchronous servo motor is shown in Figure 3. The mechanism consists of the rigid crank JA with length r, the rigid rod BC with length D, the flexible rod OB with length L, and the slider C with mass m_s. Other symbols in this figure are as follows: F, external force acting on the slider; θ, crank angle; ϕ, angle between the Y-axis and the undeformed axis of the flexible rod OB; β, angle between the X-axis and the rigid rod BC.

The deformed configuration of the quick-return mechanism is shown in Figure 4; $\boldsymbol{e}_i$ and $\boldsymbol{e}_j$ are the unit vectors of the rotating frame $Ox'y'$ which rotates with an angular velocity ϕ_t. $\boldsymbol{i}$ and $\boldsymbol{j}$ are the unit vectors of the fixed frame OXY. $x_1'(t)$ is the current position of the translating/rotating joint. The friction forces of the translating/rotating joint and slider C are neglected. The flexible quick-return mechanism considered in this study including

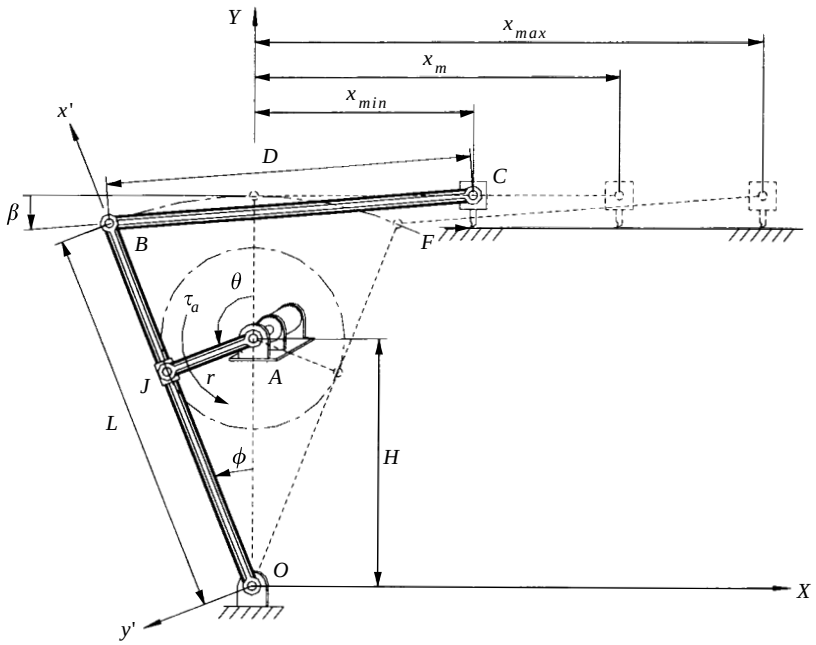

Figure 3. Quick-return mechanism before deformation.

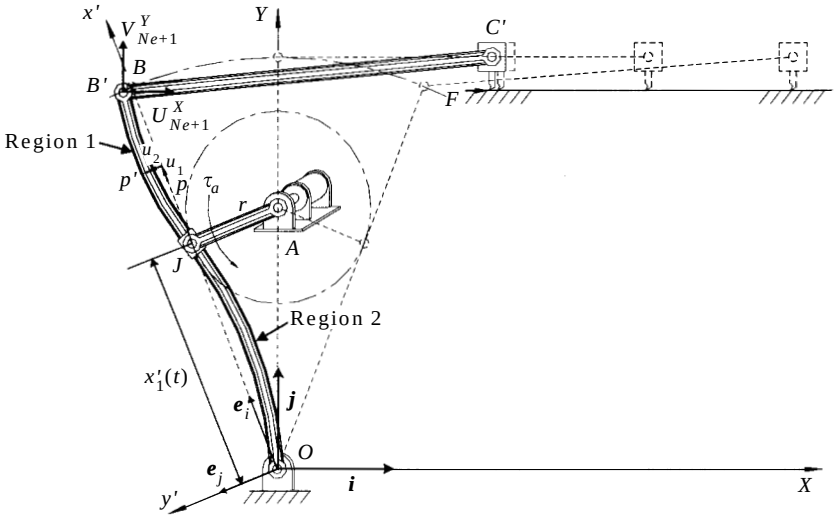

Figure 4. Deformed quick-return mechanism with a flexible connecting rod and driven by a PM synchronous servo motor.

the rigid rod BC, slider C, a reduction gear box and motor dynamics is different from those in Fung and Lee [8], Lee [4] and Beale and Scott [2] where the above elements were not considered. By adding these elements, the motor-mechanism coupled system closes to a industry prototype. In addition, those previous studies investigated the responses with constant speed of crank rotation, but in this study the dynamic formulation includes a non-constant angular velocity.

Since the translating/rotating joint moves reciprocally along the flexible rod OB, there is a time-dependent boundary involved [8]. The total length L of the flexible rod is divided into two regions as shown in Figure 4. We divide the rod into N_e elements for the finite element analysis. Regions 1 and 2 have m and n elements respectively. Thus, the total number of elements, N_e equals $m + n$. In addition, $l_1(t)$ is the element length in region 1 for $x_1'(t) \leqslant x' \leqslant L$ and $l_2(t)$ is the element length in region 2 for $0 \leqslant x' \leqslant x_1'(t)$. The element lengths of the two regions are respectively

$$l_1(t) = \frac{L - x_1'(t)}{m}, \qquad x_1'(t) \leqslant x' \leqslant L, \tag{26a}$$

$$l_2(t) = \frac{x_1'(t)}{n}, \qquad 0 \leqslant x' \leqslant x_1'(t), \tag{26b}$$

and (26a) and (26b) satisfy the relationship

$$ml_1(t) + nl_2(t) = L. \tag{27}$$

4.2. FINITE ELEMENT FORMULATION

The displacement field of the flexible rod modelled by Timoshenko beam theory is

$$u_1(x, y, t) = u(x, t) - y\psi(x, t),$$
$$u_2(x, y, t) = v(x, t), \tag{28}$$

where u and v represent the axial and transverse displacements of the flexible rod respectively, and ψ is the slope of the deflection curve due to bending deformation alone.

In this paper, we select the rotating coordinate system $Ox'y'$ fixed on the flexible connecting rod to be the reference coordinate. Figure 5 shows the ith beam element undergoing gross motion and elastic deformation. The deformed position vector of an arbitrary point P in the ith element is

$$\boldsymbol{R}(x, y, t) = (R^i(t) + x + u_1)\boldsymbol{e}_i + u_2\boldsymbol{e}_j, \tag{29}$$

where vector $R^i(t)\boldsymbol{e}_i$ locates the origin o' of the local coordinate system $o'xy$ of the ith beam element. Thus, the length $R^i(t)$ in regions 1 and 2 are respectively

$$R^i(t) = \begin{cases} nl_2(t) + (i-1)l_1(t), & i = 1, 2, \ldots, m; \\ (i-1)l_2(t), & i = 1, 2, \ldots, n. \end{cases} \tag{30}$$

Two independent holomonic constraint equations of the quick-return mechanism are

$$\boldsymbol{\Phi}(\boldsymbol{Q}) = \begin{bmatrix} \sin\phi(H + r\cos\theta) - r\sin\theta\cos\phi \\ D\sin\beta - L(1-\cos\phi) \end{bmatrix} = \boldsymbol{0}, \tag{31}$$

where $\mathbf{Q} = [\phi, \beta, \theta, u_1, v_1, \psi_1, \ldots, u_{N_e+1}, v_{N_e+1}, \psi_{N_e+1}]^T$ is the vector of generalized coordinates.

The kinematic velocity and acceleration equations are obtained by taking the first and second derivatives of (31), respectively, as

$$\boldsymbol{\Phi}_Q\dot{\boldsymbol{Q}} = \begin{bmatrix} \dot\phi(H\cos\phi + r\cos(\theta-\phi)) - r\dot\theta\cos(\theta-\phi) \\ D\dot\beta\cos\beta - L\dot\phi\sin\phi \end{bmatrix} = \boldsymbol{0}, \tag{32}$$

$$\boldsymbol{\Phi}_Q\ddot{\boldsymbol{Q}} = \begin{bmatrix} -r(\dot\theta-\dot\phi)^2\sin(\theta-\phi) + H\dot\phi^2\sin\phi \\ D\beta^2\sin\beta + L\dot\phi^2\cos\phi \end{bmatrix} = \boldsymbol{\gamma}. \tag{33}$$

Then, by differentiating (29) with respect to time t, the absolute velocity vector is

$$\boldsymbol{R}_t(x, y, t) = (R_i^i(t) + u_t - y\psi_t - v\phi_t)\boldsymbol{e}_i + ((R^i(t) + x + u - y\psi)\phi_t + v_t)\boldsymbol{e}_j. \tag{34}$$

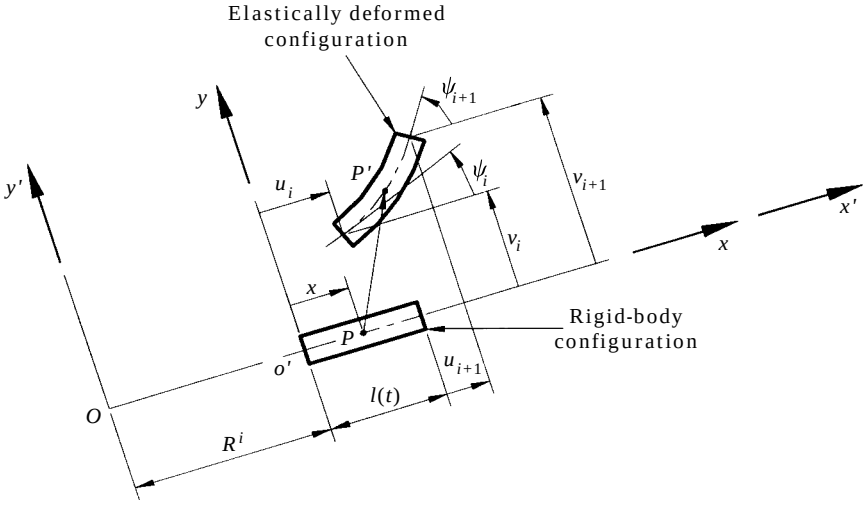

Figure 5. The ith beam element undergoing gross motion and elastic deformation.

The kinetic energy for the ith element is given by

$$T_i = \tfrac{1}{2}\int_{V_e} \boldsymbol{R}_t \cdot \boldsymbol{R}_t \, \mathrm{d}V_e$$

$$= \tfrac{1}{2}\int_0^{l(t)} \{\rho A\{[R_t^i + u_t - v\phi_t]^2 + [(R^i + x + u)\phi_t + v_t]^2\} + \rho I(\psi_t^2 + \phi_t^2\psi^2)\} \, \mathrm{d}x, \tag{35}$$

where $l(t)$ denotes the element length $l_1(t)$ in region 1 and the element length $l_2(t)$ in region 2. The Lagrange strains are

$$\varepsilon_{xx} = u_x - y\psi_x, \qquad \varepsilon_{yy} = 0, \qquad \varepsilon_{xy} = \tfrac{1}{2}(v_x - \psi), \tag{36}$$

where the high order terms $\frac{1}{2}\psi^2$, $u_x\psi$ and $y\psi\psi_x$ are neglected. The strain energy for the ith element due to bending, axial and shear deformations is

$$U_i = \tfrac{1}{2}\int_{V_e} \sigma_{ij}\epsilon_{ij} \, \mathrm{d}V_e$$

$$= \tfrac{1}{2}\int_0^{l(t)} \{EAu_x^2 + EI\psi_x^2 + KGA(v_x - \psi)^2\} \, \mathrm{d}x. \tag{37}$$

The kinetic energy of crank with mass m_c and moment of inertia $I_{c,CG}$ is

$$T_c = \tfrac{1}{2}I_{c,CG}\dot{\theta}^2 = \tfrac{1}{6}m_c r^2\dot{\theta}^2, \tag{38}$$

The kinetic energy of the rigid rod BC with mass m_r and moment of inertia $I_{r,CG}$ is

$$\begin{aligned} T_r &= \tfrac{1}{2}(m_r\dot{X}_{r,CG}^2 + m_r\dot{Y}_{r,CG}^2 + I_{r,CG}\dot{\beta}^2) \\ &= \tfrac{1}{2}m_r\{\tfrac{1}{3}D^2\dot{\beta}^2 + DL\dot{\beta}\dot{\phi}\sin\beta\cos\phi + L^2\dot{\phi}^2\cos^2\phi + \{\dot{q}\}_{N_e+1}^T([m_u]^T[m_u] \\ &\quad + [m_v]^T[m_v])\{\dot{q}\}_{N_e+1} + 2\{\dot{q}\}_{N_e+1}^T([\dot{m}_v]^T[m_v] + [\dot{m}_u]^T[m_u])\{q\}_{N_e+1} \\ &\quad + \{q\}_{N_e+1}^T([\dot{m}_u]^T[\dot{m}_u] + [\dot{m}_v]^T[\dot{m}_v])\{q\}_{N_e+1} - \{D\dot{\beta}(\cos\beta[m_v] + \sin\beta[m_u]) \\ &\quad + 2L\dot{\phi}\cos\phi[m_u]\}\{\dot{q}\}_{N_e+1} - \{D\dot{\beta}\cos\beta[\dot{m}_v] + D\dot{\beta}\sin\beta[\dot{m}_u] \\ &\quad + 2L\dot{\phi}\cos\phi[\dot{m}_u]\}\{q\}_{N_e+1}\}, \end{aligned} \tag{39}$$

where

$$X_{r,CG} = -L\sin\phi + \frac{D}{2}\cos\beta + U_{N_e+1}^X, \qquad Y_{r,CG} = -\frac{D}{2}\sin\beta + V_{N_e+1}^Y,$$

$$I_{r,CG} = \tfrac{1}{12}m_r D^2,$$

$$U_{N_e+1}^X = [m_u]\{q\}_{N_e+1} = [-\sin\phi \quad -\cos\phi \quad 0]\begin{bmatrix} u_{N_e+1} \\ v_{N_e+1} \\ \psi_{N_e+1} \end{bmatrix},$$

$$V_{N_e+1}^Y = [m_v]\{q\}_{N_e+1} = [\cos\phi \quad -\sin\phi \quad 0]\begin{bmatrix} u_{N_e+1} \\ v_{N_e+1} \\ \psi_{N_e+1} \end{bmatrix}.$$

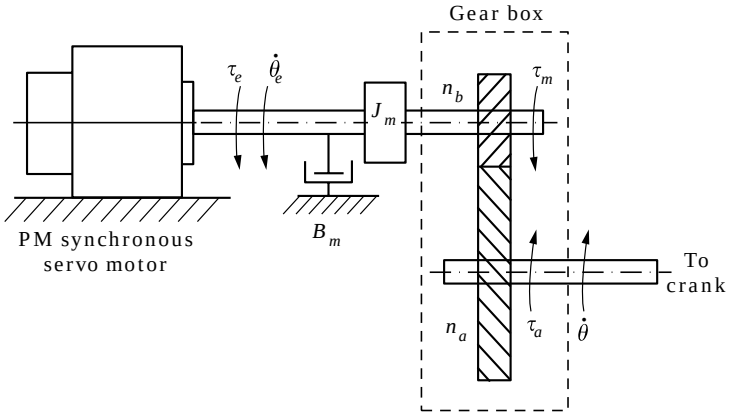

Figure 6. Schematic of the motor-gear-mechanism.

The kinetic energy of the slider with mass m_s is

$$\begin{aligned} T_s &= \tfrac{1}{2} m_s \dot{X}_{s,CG}^2 \\ &= \tfrac{1}{2} m_s \{(D\dot{\beta} \sin\beta + L\dot{\phi} \cos\phi)^2 + \{\dot{q}\}_{N_e+1}^T [m_u]^T [m_u] \{\dot{q}\}_{N_e+1} \\ &\quad + \{q\}_{N_e+1}^T [\dot{m}_u]^T [\dot{m}_u] \{q\}_{N_e+1} + 2\{\dot{q}\}_{N_e+1}^T [\dot{m}_u]^T [m_u] \{q\}_{N_e+1} \\ &\quad - 2(D\beta \sin\beta [m_u] + L\dot{\phi} \cos\phi [m_u] \{\dot{q}\}_{N_e+1} \\ &\quad - 2(D\dot{\beta} \sin\beta [\dot{m}_u] + L\dot{\phi} \cos\phi [\dot{m}_u]) \{q\}_{N_e+1}\}, \end{aligned} \tag{40}$$

where $X_{s,CG} = D \cos\beta - L \sin\phi + U_{N_e+1}^x$.

Figure 6 shows a PM synchronous servo motor system including a gear reduction set and an output torque is applied to the flexible quick-return mechanism. It is noted that g_r is the gear ratio, K_t is the motor torque constant, J_m is the rotor moment of inertia and B_m is the damping factor. The virtual works done by the external force F applied on the slider C, and the driving torque τ_a applied on the crank [25] are

$$\begin{aligned} \delta W^A &= F\delta X_{s,CG} + \tau_a \delta\theta \\ &= F(-D \sin\beta)\delta\beta + F(-L \cos\phi)\delta\phi + F[m_u]\delta\{q\}_{N_e+1} \\ &\quad + g_r(K_t i_q^* - g_r J_m \theta_{tt} - g_r B_m \theta_t)\delta\theta. \end{aligned} \tag{41}$$

The generalized constraint reaction force can be obtained in term of Lagrange multiplier $\boldsymbol{\lambda}$ as:

$$\boldsymbol{F}^C = \boldsymbol{\Phi}_Q^T \boldsymbol{\lambda},$$

where

$$\boldsymbol{\Phi}_Q = \begin{bmatrix} H\cos\phi + r\cos(\theta-\phi) & 0 & -r\cos(\theta-\phi) & \mathbf{0} \\ -L\sin\phi & D\cos\beta & 0 & \mathbf{0} \end{bmatrix}. \tag{42}$$

Thus, the virtual works by all constraint reaction forces are

$$\delta W^C = \delta \boldsymbol{Q}^T \boldsymbol{F}^C. \tag{43}$$

In the FEM, it is assumed that each unknown deformation $w(x, t)$ is approximated by a finite series in the following form

$$w(x, t) = \sum_{i=1}^{N_e+1} N_i(x, l(t))q_i(t), \tag{44}$$

where $N_e + 1$ is the total number of nodal points, $q_i(t)$ represents the nodal displacement, and $N_i(x, l(t))$ is a function of x and $l(t)$. The finite series (44) permits the evaluations of the integrals in (35) and (37), and the Lagrangian function becomes a function of the unknown nodal displacement $q_i(t)$ and time-dependent element length $l(t)$.

To provide continuity at the intersections of the finite elements, three nodal deflections at each end of an element will be introduced. The displacements at each node point are assumed to be composed of the axial deformation u, transverse deformation v and rotation ψ. The choice of the function $N_i(x, l(t))$ has a significant effect on the accuracy of the solutions.

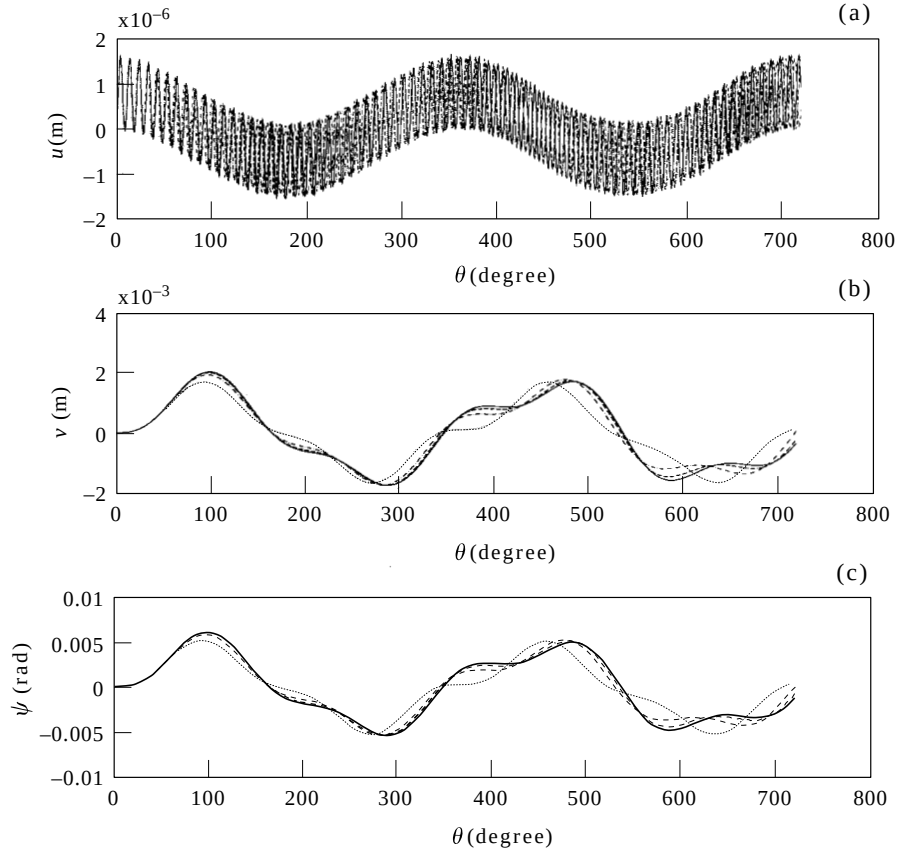

Figure 7. Comparison responses between two, four, six and eight elements with $\dot{\theta} = 100$ rad/s. (a) Axial deflection u, (b) transverse deflection v, (c) rotary slope ψ (eight elements ——, six elements, – – –, four elements – · –, two elements ·····).

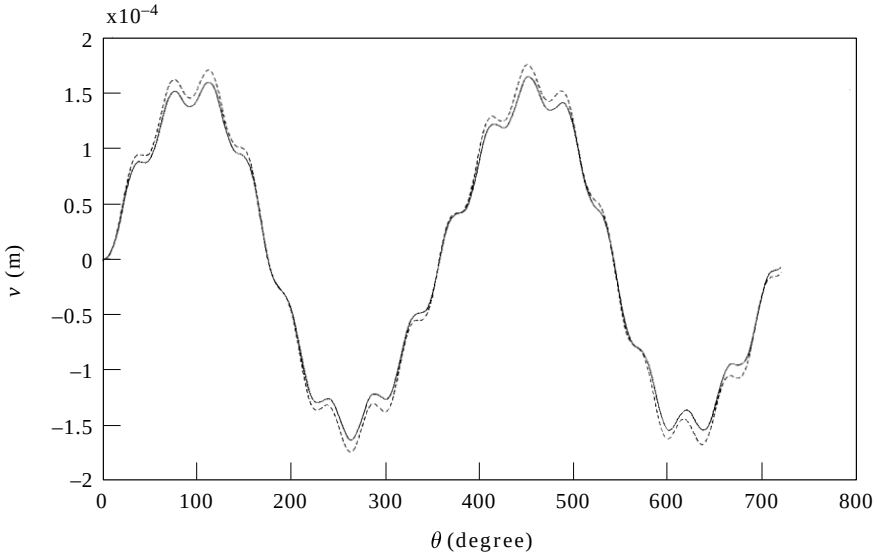

Figure 8. Transverse deformations at point B with $m_r = m_s = 0$ and $\dot{\theta} = 100$ rad/s. (Beale and Scott [2] ——, present work with six elements – – –).

In this paper, Hermite polynomials are selected to represent the functions $N_i(x, l(t))$ which is the same as in Bahgat and Willmert [5]. The unknown deformations u, v and ψ are approximated as follows:

$$\begin{Bmatrix} u \\ v \\ \psi \end{Bmatrix} = \begin{bmatrix} N_{u1} & 0 & 0 & N_{u2} & 0 & 0 \\ 0 & N_{v1} & N_{v2} & 0 & N_{v3} & N_{v4} \\ 0 & N_{\psi 1} & N_{\psi 2} & 0 & N_{\psi 3} & N_{\psi 4} \end{bmatrix} \{q\}_i = \begin{bmatrix} \boldsymbol{N}_u \\ \boldsymbol{N}_v \\ \boldsymbol{N}_\psi \end{bmatrix} \{q\}_i, \tag{45}$$

where $\{q\}_i = [u_i, v_i, \psi_i, u_{i+1}, v_{i+1}, \psi_{i+1}]^T$ is the nodal displacement vector for the ith element, and $N_{u1}, N_{u2}, \ldots, N_{v3}, N_{v4}, \ldots, N_{\psi 3}, N_{\psi_4}$ are the general Hermite polynomials. Details of the shape functions are given in Fung and Lee [8]. It should be noted that these shape functions are time-dependent.

The derivatives of u and v and the curvature κ_c within the ith element can be written as

$$u_x = \frac{\mathrm{d}u}{\mathrm{d}x} \equiv [B_u]\{q\}_i, \qquad \kappa_c = \psi_x = \frac{\mathrm{d}\psi}{\mathrm{d}x} \equiv [B_b]\{q\}_i, \qquad v_x = \frac{\mathrm{d}v}{\mathrm{d}x} \equiv [B_v]\{q\}_i \quad \text{(46a, b, c)}$$

where

$$[B_u] = \frac{\mathrm{d}}{\mathrm{d}x}[N_u], \qquad [B_b] = \frac{\mathrm{d}}{\mathrm{d}x}[N_\psi], \qquad [B_v] = \frac{\mathrm{d}}{\mathrm{d}x}[N_v].$$

Substituting the shape functions into the kinetic energy (35) and the strain energy (37), T_i and U_i can be rewritten in terms of the nodal displacement $\{q\}_i$. For the details see [26].

4.3. HAMILTON'S PRINCIPLE

Since there is a translating/rotating joint involved, the element length, mass and stiffness matrices are time-dependent. Hamilton's principle is

$$\int_{t_1}^{t_2} (\delta L_f + \delta W)\, \mathrm{d}t = 0, \tag{47}$$

where the virtual work is $\delta W = \delta W^A + \delta W^C$, and the Lagrangian density is

$$L_f = \sum_{i=1}^{N_e} (T_i - U_i) + T_c + T_r + T_s$$

and N_e is the total number of elements of the flexible rod. Taking variation on the Lagrangian density and combining regions 1 and 2, we obtain the global ordinary differential equation (7). The elements of $\boldsymbol{M}$, $\boldsymbol{N}$, $\boldsymbol{\Phi}_Q$, $\boldsymbol{B}$ and $\boldsymbol{U}$ are given in Appendix A.

Equations (8) and (31) may be recorded and partitioned according to the decomposition of $\mathbf{Q}$. If the constraints are independent, matrix $\boldsymbol{\Phi}_Q$ has full row rank, and there is always at least one nonsingular submatrix $\boldsymbol{\Phi}_Q$ of rank 3. Gauss–Jordan reduction of the matrix $\boldsymbol{\Phi}_Q$ with double pivoting defines a partitioning of $\mathbf{Q} = [\mathbf{p}^T, \mathbf{q}^T]^T$, $\mathbf{p} = [\phi, \beta]^T$, $\mathbf{q} = [\theta, \mathbf{u}_1, \mathbf{v}_1, \psi_1, \ldots, \mathbf{u}_{N_e+1}, \mathbf{v}_{N_e+1}, \psi_{N_e+1}]^T$ such that $\boldsymbol{\Phi}_p$ is a submatrix of $\boldsymbol{\Phi}_Q$ whose columns correspond to elements $\boldsymbol{p}$ of $\boldsymbol{Q}$ and $\boldsymbol{\Phi}_q$ is a submatrix of $\boldsymbol{\Phi}_Q$ whose columns correspond to element $\boldsymbol{q}$ of $\boldsymbol{Q}$. The elements of the vectors, $\boldsymbol{p}$, $\boldsymbol{q}$ and matrices $\boldsymbol{\Phi}_p$, $\boldsymbol{\Phi}_q$ are detailed in Appendix B.

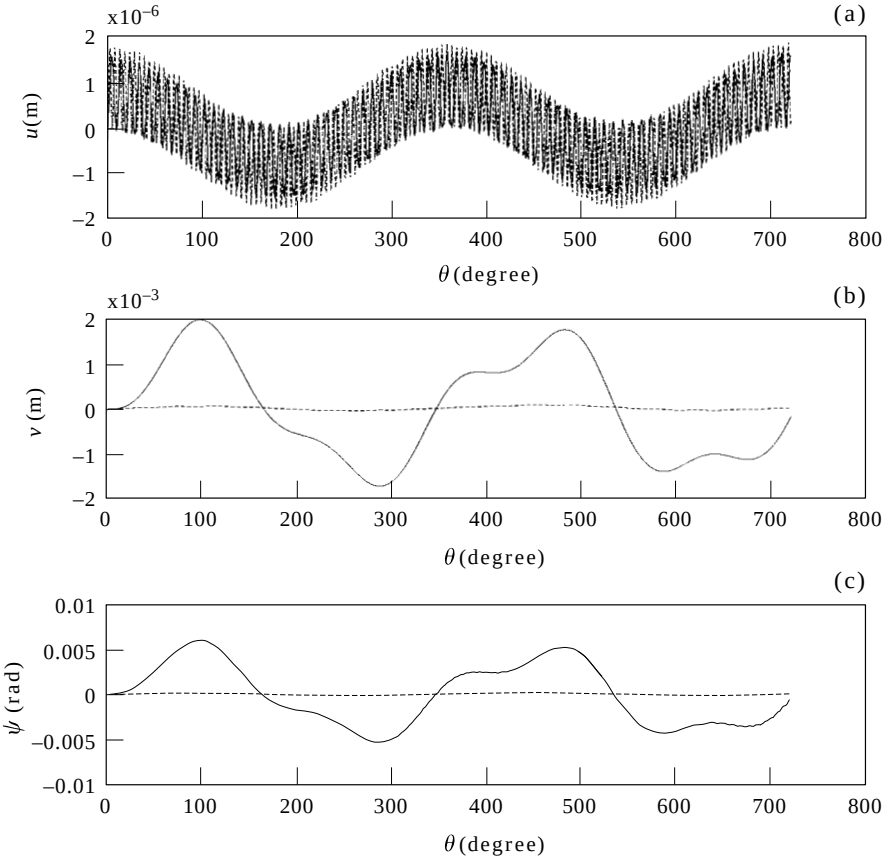

Figure 9. Inertia effects of both rigid link BC and slider C on the deflections for $\dot{\theta} = 100$ rad/s. (a) Axial deflection u, (b) transverse deflection v, (c) rotary slope ψ ($m_r = 8{\cdot}58$ kg, $m_s = 0.5$ kg ——; $m_r = m_s = 0$ ——).

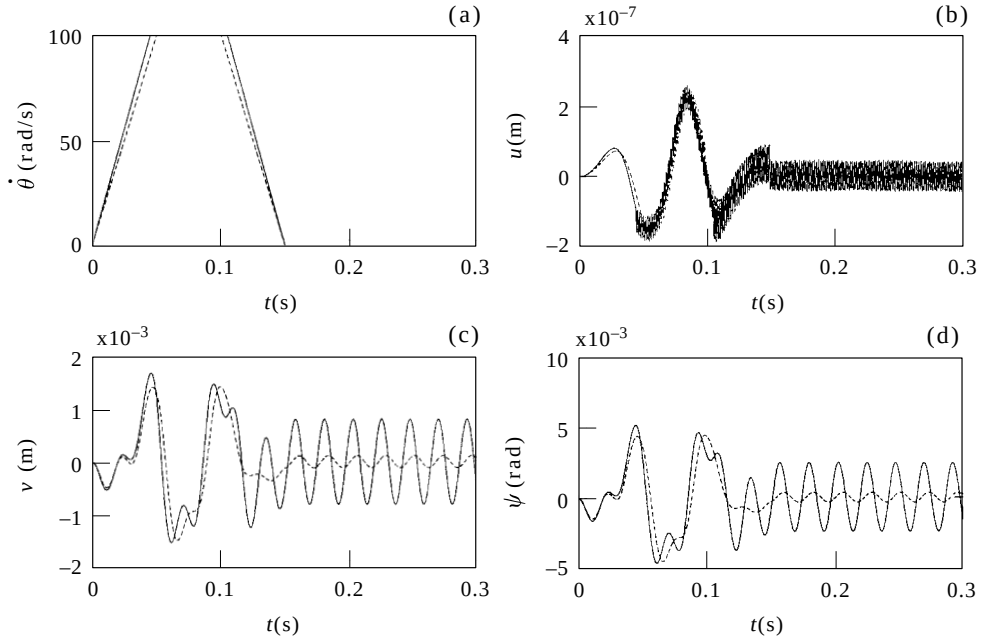

Figure 10. Transient displacements at point B of the flexible rod for a prescribed trapezoidal angular velocity. (a) Angular velocity $\dot{\theta}$, (b) axial deflection u, (c) transverse deflection v, (d) rotary slope ψ (Case 1 ——, Case 2 – – –).

5. NUMERICAL RESULTS AND DISCUSSIONS

In the numerical results, we take the same material properties and dimensions of the flexible rod as in [2]. The flexible quick-return mechanism has the following dimensions and properties:

$$L = 1\text{ m}, \quad H = 0{\cdot}59997\text{ m}, \quad r/H = 0{\cdot}01, \quad D = 1{\cdot}2\text{ m}, \quad K = 0{\cdot}886,$$

$$G = 80 \times 10^9\text{ N/m}^2, \quad E = 0{\cdot}7 \times 10^{11}\text{ N/m}^2, \quad I = 0{\cdot}5208 \times 10^{-6}\text{ m}^4, \quad d = 0{\cdot}05\text{ m},$$

$$\rho A = 7{\cdot}15\text{ kg/m}, \quad m_r = 8{\cdot}58\text{ kg}, \quad m_c = 0{\cdot}04290\text{ kg}, \quad m_s = 0{\cdot}5\text{ kg}, \quad \Delta = 0{\cdot}5$$

and the parameters of the PM synchronous servo motor are

$$K_t = 0{\cdot}6732\text{ N} \cdot \text{m/A}, \quad J_m = 1{\cdot}32 \times 10^{-3}\text{ N} \cdot \text{m} \cdot \text{s}^2, \quad B_m = 5{\cdot}78 \times 10^{-3}\text{ N} \cdot \text{m} \cdot \text{s/rad}.$$

By using the Runge–Kutta fourth-order numerical integration method, (11) is solved for the motor-mechanism coupled system. The following numerical analysis includes two parts: the constant angular velocity and trapezoidal shape angular velocity.

5.1. DYNAMIC ANALYSIS OF THE FLEXIBLE QUICK-RETURN MECHANISM

5.1.1. *Constant angular velocity*

The results in Figure 7(a)–(c) show the axial deformation, transverse deformation and rotary slope at point B. Numbers of elements are chosen as eight (solid line), six (dash line), four (dash-dotted line) and two (dotted line) elements. Here, the crank rotates with a constant angular velocity $\dot{\theta} = 100$ rad/s. The initial conditions are $\theta(0) = 0$, $\dot{\theta}(0) = 100$ rad/s and $\{q\}_i = \{\dot{q}\}_i = 0$. It is seen that four-element approximation captures most of the deflection, and six- and eight-element approximations are very close. Based

on this result, six-element approximation has the sufficient accuracy for the purpose of the following dynamic analysis and vibration control.

The dash line shown in Figure 8 is obtained by taking $m_r = m_s = 0$ kg, i.e. the rigid link BC and slider C are not considered. The present results of the flexible Timoshenko beam with six-element approximation are compared with those obtained by Beale and Scott [2], in which the Euler beam theory was employed and Galerkin's method was used for the first three modes solutions. It is seen that the results of the Timoshenko beam theory are larger than those of the Euler beam theory.

Figure 9(a)–(c) show the effects of the rigid link BC and slider C on the flexible deformations. Since the inertia forces of both rigid link and slider cause the bending moment and shear stress in the flexible rod, a slight difference is shown in the axial deformation [Figure 9(a)], but the amplitudes are much larger in the transverse deformation [Figure 9(b)] and rotary slope [Figure 9(c)].

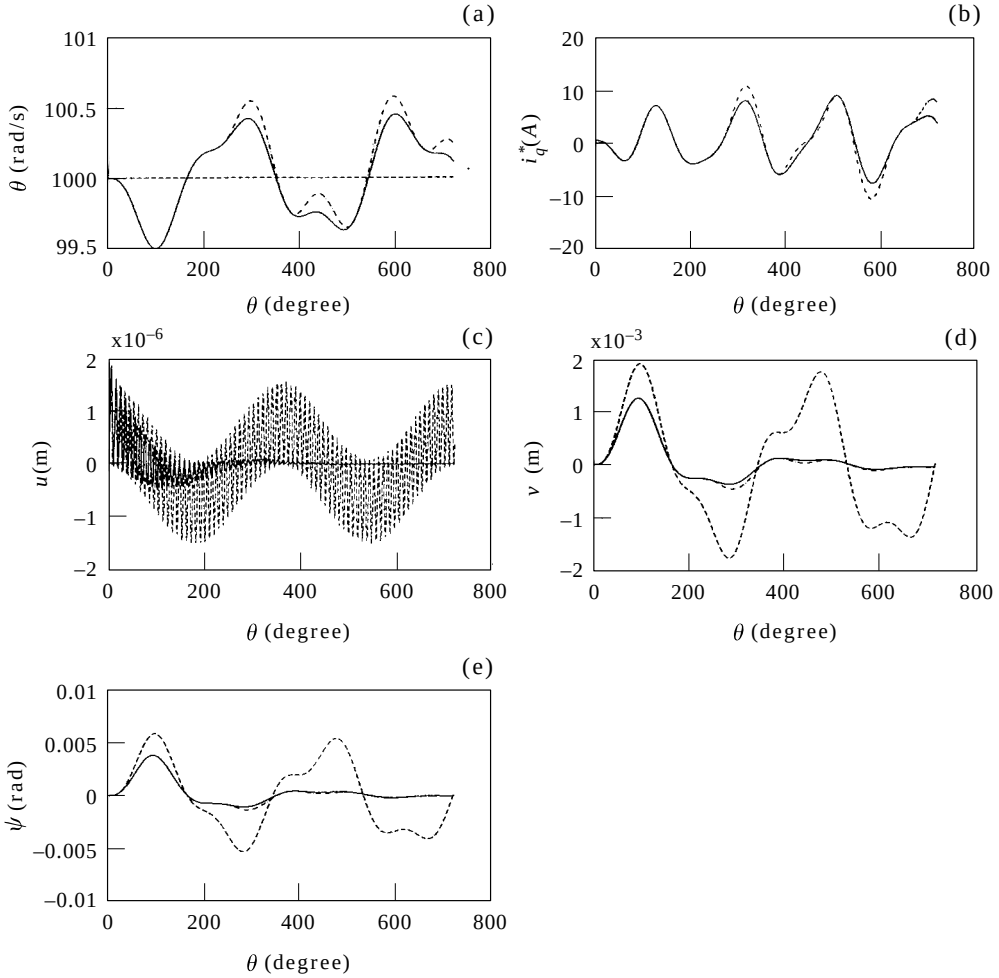

Figure 11. Constant angular velocity controlled by the proposed VSC law. (a) Angular velocity $\dot{\theta}$, (b) control input current i_q^*, (c) axial deflection u, (d) transverse deflection v, (e) rotary slope ψ [controlled ($F = 0$ N) ——, uncontrolled ($F = 0$ N) ——, controlled ($F = 196$ N during $4\pi/3 \leqslant \theta \leqslant 4\pi$) – · –·.

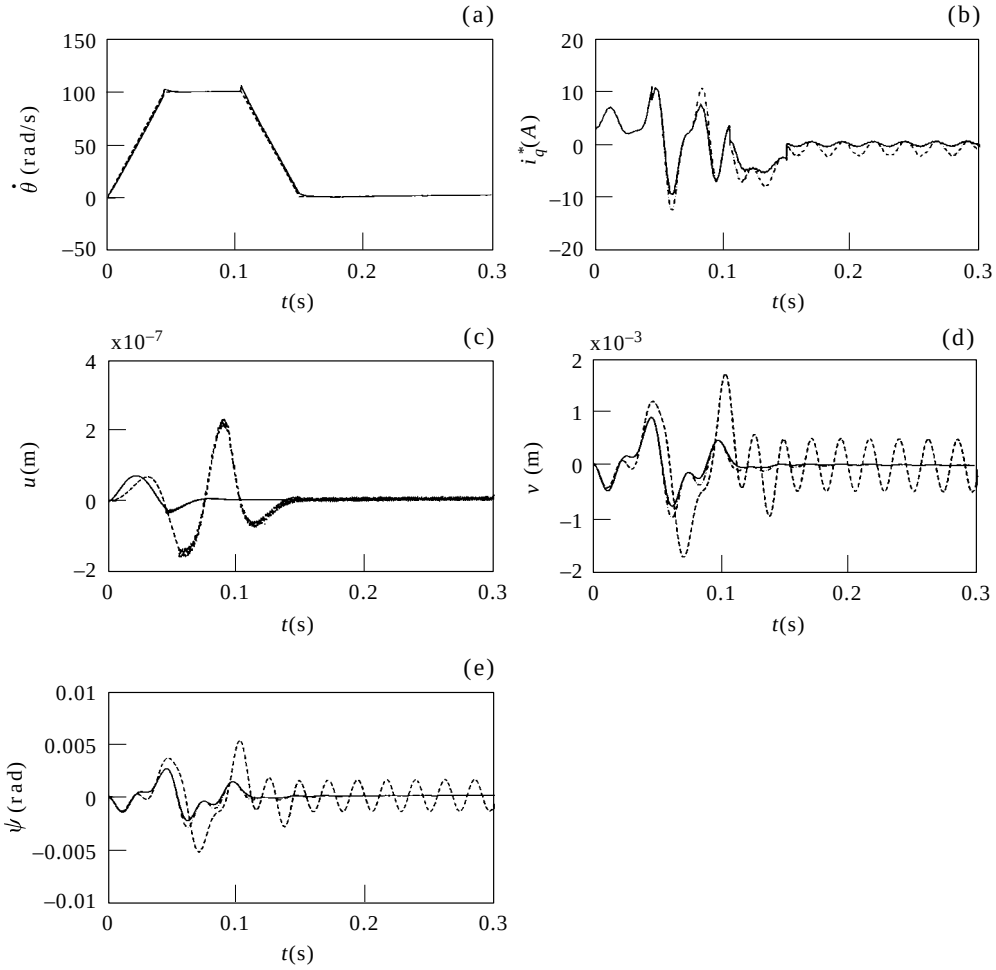

Figure 12. Transient displacements at point B of the flexible rod for a prescribed trapezoidal angular velocity. (a) Angular velocity $\dot{\theta}$, (b) control input current i_q^*, (c) axial deflection u, (d) transverse deflection v, (e) rotary slope ψ [controlled ($F = 0$ N) ——, uncontrolled ($F = 0$ N) – – –, controlled ($F = 196$ N during $4\pi/3 \leqslant \theta \leqslant 4\pi$) – · –·.

5.1.2. *Trapezoidal angular velocity*

In many cases, a motor driving body, such as a manipulator, is usually with a velocity input of the trapezoidal shape [26]. As shown in Figure 10(a), the prescribed angular velocity

$$\dot{\theta}_d(t) = \begin{cases} \dfrac{100t}{t_1}, & 0 < t \leqslant t_1 \\ 100, & t_1 < t \leqslant t_2 \\ \dfrac{100(t - t_3)}{(t_2 - t_3)}, & t_2 < t \leqslant t_3 \\ 0 & t_3 < t \end{cases},$$

is the trapezoidal angular velocity for the crank rotating. The initial conditions are $\boldsymbol{p}(0) = \dot{\boldsymbol{p}}(0) = \boldsymbol{q}(0) = \dot{\boldsymbol{q}}(0) = \boldsymbol{0}$. Figure 10(a)–(d) show the different results between Case 1:

$t_1 = 0{\cdot}045$, $t_2 = 0{\cdot}105$, $t_3 = 0{\cdot}15$ (solid line) and Case 2: $t_1 = 0{\cdot}05$, $t_2 = 0{\cdot}10$, $t_3 = 0{\cdot}15$ (dash line). Because Case 1 has a faster speed up and down in the accelerating and decelerating processes, it is observed that the vibration amplitudes of Case 1 are larger than those of Case 2, whether in the accelerating, constant speed and decelerating processes. In addition, because a part of energy goes into the flexible deformations of the connecting rod OB, both Cases have the residual oscillation phenomena after 0·15 s when the crank does not rotate.

5.2. VIBRATION CONTROL OF THE FLEXIBLE QUICK-RETURN MECHANISM

Yeung and Chen [12, 13] and Chen and Yeung [27] used the pole placement method to obtain good dynamic responses of a flexible robot arms. However, their method is only applied to the linear systems associated with constant symmetry inertia matrices. In this study, non-linearity and asymmetry inertia matrices are included in the system; traditional trial-and-error method will be applied to choose gains of the control laws in the following sections. To decrease the order of the gain matrix, only four elements of the connecting rod, which captures most of the deflections, are considered in the vibration control.

5.2.1. *Constant angular velocity control*

By using a trial and error method, the gain matrices for the switching function are

$$\boldsymbol{C}_1 = [12 \quad 150 \quad 25 \quad 50 \quad 25 \quad 300 \quad 150 \quad 25 \quad 50 \quad 25 \quad 300 \quad 170 \quad 130],$$

$$\boldsymbol{C}_2 = [30 \quad 0{\cdot}5 \quad 0{\cdot}05 \quad 0{\cdot}025 \quad 0{\cdot}016 \quad 0{\cdot}4 \quad 0{\cdot}8 \quad 0{\cdot}06 \quad 0{\cdot}05 \quad 0{\cdot}036 \quad 0{\cdot}12 \quad 0{\cdot}6 \quad 0{\cdot}2],$$

and $P = 2{\cdot}5$, $Q = 0{\cdot}5$ and $\kappa = 0{\cdot}3$. In Figure 11(a) and (b), the solid lines show the transient responses of the crank angular velocity and the control input current respectively. It is seen that the angular velocity has a slightly shift of $\pm 0{\cdot}5$ rad/s about the reference angular velocity of 100 rad/s for reducing the vibration. Because the saturation function (25) is used in the control law, the current input shown in Figure 11(b) is smooth without the chattering phenomenon. In Figure 11(c)–(e), it is shown that the proposed VSC law decreases the longitudinal and transverse deflections and rotary slope at point B (solid lines) asymptotically. The dash-dotted lines in Figures 11(a)–(e) are obtained by applying an external disturbance ($F = 196$ N) during $4\pi/3 \leqslant \theta \leqslant 4\pi$. In Figure 11(a) the angular velocity response is robust with the rejection of disturbance, but a larger current input i_q^* during $4\pi/3 \leqslant \theta \leqslant 4\pi$ is shown in Figure 11(b). The vibration amplitudes in Figure 11(c)–(e) are also diminished asymptotically. Thus, the proposed controller is robust for rejection disturbances.

5.2.2. *Trapezoidal angular velocity control*

The desired trapezoidal angular velocity is assumed the same as in Case 1 of Section 5.1.2. The gain matrices for the switching surface are

$$\boldsymbol{C}_i = [500 \quad 0{\cdot}2 \quad 2 \quad 0{\cdot}2 \quad 0{\cdot}4 \quad 20 \quad 0{\cdot}6 \quad 3 \quad 0{\cdot}2 \quad 0{\cdot}4 \quad 25 \quad 16 \quad 8],$$

$$\boldsymbol{C}_j = [100 \quad 0{\cdot}4 \quad 1 \quad 0{\cdot}1 \quad 0{\cdot}05 \quad 2{\cdot}4 \quad 1 \quad 0{\cdot}2 \quad 0{\cdot}1 \quad 0{\cdot}05 \quad 1{\cdot}2 \quad 0{\cdot}04 \quad 0{\cdot}02],$$

$P = 150$, $Q = 25$ and $\kappa = 0{\cdot}3$. The transient responses (dash line, without control) of the desired trapezoidal angular velocity are shown in Figure 12(a). In order to suppress the deflections in Figure 12(c)–(e) (solid lines for the control system), the control input currents i_q^* in Figure 12(b) have the chattering and oscillating phenomena after $t > 0{\cdot}15$ s. The dash-dotted lines in Figure 12(a)–(e) are obtained by adding the external disturbance ($F = 196$ N) applied during $0{\cdot}05 \leqslant t \leqslant 0{\cdot}3$ s. In order to reject the disturbances, the control input current in Figure 12(b) is larger than that without the disturbance. It is obvious that

the higher control input provides the higher torque to the mechanism during impacting disturbance. The transient deflections in Figure 12(c)–(e) are larger as compared with those without disturbances. Consequently, all deflections converge to zero asymptotically. Thus, the proposed controller scheme for the trapezoidal angular velocity control is also robust to the external disturbances.

6. CONCLUSION

The flexible rod of a quick-return mechanism driven by a PM synchronous servo motor is modelled by the Timoshenko beam theory. The finite element method and Hamilton's principle are employed to derive the governing equations in the matrix form. When the crank rotates, the induced vibrations occur in the flexible connecting rod. To suppress the vibrations, we have successfully designed a reaching law variable structure control method. The distinctive results of this study are summarized as follows.

(1) The controller, motor and flexible quick-return mechanism coupled system has been derived completely with the crank operating at a non-constant speed.
(2) The design procedure of vibration control can also be applied to any other motor-mechanism coupled system. The more the number of elements is chosen, the more the order of the gain matrix is needed.
(3) The design procedure of VSC is simple. Numerical results have shown that the proposed VSC not only eliminates deflectons of the flexible connecting rod, but also keeps good performances.
(4) Robust control performances of the controller–motor–mechanism coupled systems are obtained by the proposed controllers with respect to the external disturbances.

ACKNOWLEDGMENTS

The authors are greatly indebted to the National Science Council R.O.C. for the support of the through contract No. NSC 84-2212-E-033-009 and Chung Yuan Christian University with contract No. CY 85-RG-004.

REFERENCES

1. S. N. Dwivedi 1984 *Mechanism and Machine Theory* **19**, 51–59. Application of Whitwork quick return mechanism for high velocity impacting press.
2. D. G. Beale and R. A. Scott 1990 *Journal of Sound and Vibration* **141**, 277–289. The stability and response of a flexible rod in a quick return mechanism.
3. D. G. Beale and R. A. Scott 1993 *Journal of Sound and Vibration* **166**, 463–476. The stability and response of a flexible rod in a quick return mechanism: large crank case.
4. H. P. Lee 1994 *Transactions of the American Society of Mechanical Engineers*, *Journal Mechanical Design* **116**, 70–74. Dynamics of a flexible rod in a quick return mechanism.
5. B. M. Bahgat and K. D. Willmert 1976 *Mechanism and Machine Theory* **11**, 47–71. Finite element vibrational analysis of planar mechanisms.
6. J. O. Song and E. J. Haug 1980 *Computer Methods in Applied Mechanics and Engineering* **24**, 359–381. Dynamic analysis of planar flexible mechanisms.
7. Z. Yang and J. P. Sadler 1990 *Transactions of the American Society of Mechanical Engineers*, *Journal of Mechanical Design* **112**, 175–182. Large-displacement finite element analysis of flexible linkages.
8. R. F. Fung and F. Y. Lee 1997 *Journal of Sound and Vibration* **202**, 187–201. Dynamic analysis of the flexible rod of a quick-return mechanism with time-dependent coefficients by the finite element method.
9. A. Shabana and B. Thomas 1987 *Mechanism and Machine Theory* **22**, 359–369. Chatter vibration of flexible multibody machine tool mechanisms.

10. W. J. Book, N. O. Maizza and D. E. Whitney 1975 *Transactions of the American Society of Mechanical Engineers*, *Journal of Dynamic System*, *Measurement and Control* **97**, 424–431. Feedback control of two beams, two joint systems with distributed flexibility.
11. A. Flcola, M. L. Cava and P. Muraca 1992 *IFAC Motion Control for Intelligent Automation Perugia*, *Italy* **October**, 27–29. A simplified strategy to implement sliding mode control of a two-joints robot with a flexible forearm.
12. K. S. Yeung and Y. P. Chen 1989 *International Journal of Control* **49**, 1965–1978. Regulation of a one-link flexible robot arm using sliding mode technique.
13. K. S. Yeung and Y. P. Chen 1990 *International Journal of Control* **52**, 101–117. Sliding-mode controller design of a single-link flexible manipulator under gravity.
14. S. B. Choi, C. C. Cheong and H. C. Shin 1995 *Journal of Sound and Vibration* **179**, 737–748. Sliding mode control of vibration in a single-link flexible arm with parameter variations.
15. B. K. Bose 1988 *Institute of Electrical and Electronic Engineers*, *Transactions on Industry Electronics* **35**, 160–176. Technology trends in microcomputer control of electrical machines.
16. P. C. Sen 1990 *Institute of Electrical and Electronic Engineers*, *Transactions on Industry Electronics* **37**, 562–575. Electric motor drives and control—past, present, and future.
17. W. Leonnard 1986 *Automatica* **22**, 1–19. Microcomputer control of high dynamic performance ac drives: a survey.
18. E. N. Parviz 1988 *Computer-Aided Analysis of Mechanical System*. Englewood Cliffs, N.J.: Prentice–Hall International. pp. 42–46.
19. J. J. Slotine and S. S. Sastry 1983 *International Journal of Control* **38**, 465–492. Tracking control of nonlinear systems using sliding surface with application to robot manipulators.
20. K. W. Chen 1997 *Master Thesis in Mechanical Engineering*, *Chung-Yuan Christian University*, *Chung-Li*, *Taiwan*. Vibration analysis and variable structure control of the flexible mechanisms driven by a PM synchronous servo motor.
21. S. K. Chung, J. H. Lee, J. S. Ko and M. J. Youn 1995 *Institute of Electrical Engineering Proceedings—Electronics Power Application* **142**, 361–370. Robust speed control of brushless direct-drive motor using integral variable structure control.
22. W. Geo and J. C. Hung 1993 *Institute of Electrical and Electronic Engineers*, *Transactions on Industrial Electronics* **40**, 45–55. Variable structure control of nonlinear systems: a new approach.
23. W. J. Wang and J. L. Lee 1993 *Journal of Control Systems and Technology* **1**, 19–25. Hitting time reduction and chattering attenuation in variable structure systems.
24. U. Itkis 1976 *Control System of Variable Structure*. New York: Wiley.
25. N. Mohan, T. R. Undeland and W. P . Robbins 1989 *Power Electronics—2nd edition*. New York: Wiley.
26. T. S. Liu and J. C. Lin 1993 *Transactions of the American Society of Mechanical Engineers*, *Journal of Vibration and Acoustics* **115**, 468–476. Forced vibration of flexible body systems: a dynamic stiffness method.
27. Y. P. Chen and K. S. Yeung 1991 *International Journal of Control* **54**, 257–278. Sliding-mode control of multi-link flexible manipulator.

APPENDIX A

The elements of $\boldsymbol{M}$, $\boldsymbol{N}$, $\boldsymbol{\Phi}_Q\boldsymbol{B}$ and $\boldsymbol{U}$ are given

$$\boldsymbol{M} = \begin{bmatrix} M_{11} & M_{12} & M_{13} & M_{14} \\ M_{21} & M_{22} & M_{23} & M_{24} \\ M_{31} & M_{32} & M_{33} & M_{34} \\ M_{41} & M_{42} & M_{43} & M_{44} \end{bmatrix}, \quad \boldsymbol{N} = \begin{bmatrix} N_1 \\ N_2 \\ N_3 \\ N_4 \end{bmatrix}, \quad \boldsymbol{B} = \begin{bmatrix} 0 \\ 0 \\ -1 \\ \mathbf{0} \end{bmatrix},$$

$$\boldsymbol{\Phi}_Q = \begin{bmatrix} H\cos\phi + r\cos(\theta-\phi) & 0 & -r\cos(\theta-\phi) & \mathbf{0} \\ -L\sin\phi & D\cos\beta & 0 & \mathbf{0} \end{bmatrix}, \quad \boldsymbol{U} = [i_q^*],$$

where $\boldsymbol{M}$ is a $(4+N_e)\times(4+N_e)$ matrix, $\boldsymbol{N}$ is a $(4+N_e)\times 1$ matrix and $\boldsymbol{\Phi}_Q$ is a $2\times(4+N_e)$ matrix. M_{11}, M_{12}, M_{13}, M_{21}, M_{22}, M_{23}, M_{31}, M_{32} and M_{33} are chosen as the 1×1 matrices, $\boldsymbol{M}_{14}$, $\boldsymbol{M}_{24}$ and $\boldsymbol{M}_{34}$ are chosen as the $1\times(N_e+1)$ matrices, $\boldsymbol{M}_{41}$, $\boldsymbol{M}_{42}$, $\boldsymbol{M}_{43}$, and $\boldsymbol{N}_4$ are chosen as the $(N_e+1)\times 1$ matrices, $\boldsymbol{M}_{44}$ is a $(N_e+1)\times(N_e+1)$ matrix and

$$M_{11} = -(m_r+m_s)L^2\cos^2\phi - (\{q\}_i^T[m_{2b}]\{q\}_i + 2[m_{qa}]\{q\}_i + 2Z_r^*),$$

$$M_{12} = -(\tfrac{1}{2}m_r+m_s)DL\sin\beta\cos\phi, \qquad M_{13}=0,$$

$$[M_{13}\quad \boldsymbol{M}_{14}]\ddot{\boldsymbol{q}} = -\sum_{i=1}^{N_e}(\{q\}_i^T[m_{3a}]+[m_{qt1}])\{\ddot{q}\}_i + (m_r+m_s)L\cos\phi[m_u]\{\ddot{q}\}_{N_e+1},$$

$$M_{21} = -(\tfrac{1}{2}m_r+m_s)DL\sin\beta\cos\phi, \qquad M_{22} = -(\tfrac{1}{3}m_r+m_s\sin^2\beta)D^2, \qquad M_{23}=0,$$

$$[M_{23}\quad \boldsymbol{M}_{24}]\ddot{\boldsymbol{q}} = D\{\tfrac{1}{2}m_r(\cos\beta[m_v]+\sin\beta[m_u]) + m_s\sin\beta[m_u]\}\{\ddot{q}\}_{N_e+1},$$

$$M_{31}=M_{32}=0, \qquad M_{33} = -\tfrac{1}{3}m_e r^2 - g_r^2 J_m, \qquad \boldsymbol{M}_{34}=\boldsymbol{0},$$

$$[\boldsymbol{M}_{41}\quad \boldsymbol{M}_{42}]\ddot{\boldsymbol{p}} = -(m_r+m_s)L\cos\phi[m_u]^T\{\ddot{\phi}\}_{N_e+1} - \left\{\frac{m_r}{2}D(\cos\beta[m_v]^T+\sin\beta[m_u]^T) + m_sD\sin\beta[m_u]^T\right\}\{\ddot{\beta}\}_{N_e+1},$$

$$\boldsymbol{M}_{43}=\boldsymbol{0},$$

$$[\boldsymbol{M}_{43}\quad \boldsymbol{M}_{44}]\ddot{\boldsymbol{q}} = \sum_{i=1}^{N_e}[m_1]\{\ddot{q}\}_i + \{m_r([m_u]^T[m_u]+[m_v]^T[m_v]) + m_s[m_u]^T[m_u]\}\{\ddot{q}\}_{N_e+1},$$

$$\begin{aligned}N_1 = \sum_{i=1}^{N_e}\{&(m_r+m_s)L^2\dot{\phi}^2\cos\phi\sin\phi - (\tfrac{1}{2}m_r+m_s)DL\dot{\beta}^2\cos\beta\cos\phi - \{\dot{q}\}_i^T[m_{3a}]\{\dot{q}\}_i\\ &- \{\dot{q}\}_i^T(\tfrac{1}{2}[m_{2a}]+\dot{\phi}[m_{2b}])\{q\}_i - \{q\}_i^T(\tfrac{1}{2}[m_{2a}]+\dot{\phi}[m_{2b}]+[\dot{m}_{3a}])\{\dot{q}\}_i\\ &- \{q\}_i^T(\tfrac{1}{2}[\dot{m}_{2a}]+\dot{\phi}[m_{2b}])\{q\}_i - ([\dot{m}_{qt1}]+2\dot{\phi}[m_{qa}]+[m_{qb}])\{\dot{q}\}_i\\ &- (2\dot{\phi}[\dot{m}_{qa}]+[\dot{m}_{qb}])\{q\}_i\} - 2\dot{\phi}Z_r^* - FL\cos\phi + 2(m_r+m_s)L\cos\phi[\dot{m}_u]\{\dot{q}\}_{N_e+1}\\ &+ (m_r+m_s)L\cos\phi[\ddot{m}_u]\{q\}_{N_e+1},\end{aligned}$$

$$\begin{aligned}N_2 = {}&(\tfrac{1}{2}m_r+m_s)DL\dot{\phi}^2\sin\beta\sin\phi - m_sD^2\dot{\beta}^2\sin\beta\cos\beta - FD\sin\beta\\ &+ \{m_rD(\cos\beta[\dot{m}_v]+\sin\beta[\dot{m}_u]) + 2m_sD\sin\beta[\dot{m}_u]\}\{\dot{q}\}_{N_e+1}\\ &+ \{\tfrac{1}{2}m_rD(\cos\beta[\ddot{m}_v]+\sin\beta[\ddot{m}_u]) + m_s\sin\beta[\ddot{m}_u]\}\{q\}_{N_e+1},\end{aligned}$$

$$N_3 = -g_r^2B_m\dot{\theta},$$

$$\begin{aligned}\boldsymbol{N}_4 = \sum_{i=1}^{N_s}&\{([\dot{m}_1]+[m_3]^T-[m_3])\{\dot{q}\}_i + ([\dot{m}_3]-[m_2]+[K_a])\{q\}_i\} + [\dot{m}_{qt}]^T - [m_q]^T\\ &+ \{2m_r([\dot{m}_v]^T[m_v]+[\dot{m}_u]^T[m_u]) + 2m_s[\dot{m}_u]^T[m_u]\}\{\dot{q}\}_{N_e+1} + \{m_r([\ddot{m}_v]^T[m_v]\\ &+ [\ddot{m}_u]^T[m_u]) + m_s[\ddot{m}_u]^T[m_u]\}\{q\}_{N_e+1} + L(m_r+m_s)\sin\phi[m_u]^T\{\dot{\phi}\}_{N_e+1}^2\\ &+ \left\{\frac{m_r}{2}D(\sin\beta[(m_v]^T-\cos\beta[m_u]^T) - m_sD\cos\beta[m_u]^T\right\}\{\dot{\beta}\}_{N_e+1}^2 - F[m_u]^T.\end{aligned}$$

APPENDIX B

Choose $\boldsymbol{p} = [\phi \quad \beta]^T$, $\boldsymbol{q} = [\theta \quad u_1 \quad v_1 \quad \psi_1 \quad \cdots \quad u_{N_e+1} \quad v_{N_e+1} \quad \psi_{N_e+1}]^T$ and

$$\boldsymbol{\Phi}_p = \begin{bmatrix} H\cos\phi + r\cos(\theta-\phi) & 0 \\ -L\sin\phi & D\cos\beta \end{bmatrix}, \qquad \boldsymbol{\Phi}_q = \begin{bmatrix} -r\cos(\theta-\phi) & \mathbf{0} \\ 0 & \mathbf{0} \end{bmatrix}.$$

The entries of matrices in (9) are

$$\boldsymbol{M}^{pp} = \begin{bmatrix} M_{11} & M_{12} \\ M_{21} & M_{22} \end{bmatrix}, \qquad \boldsymbol{M}^{pq} = \begin{bmatrix} M_{13} & \boldsymbol{M}_{14} \\ M_{23} & \boldsymbol{M}_{24} \end{bmatrix}, \qquad \boldsymbol{M}^{qp} = \begin{bmatrix} M_{31} & M_{32} \\ \boldsymbol{M}_{41} & \boldsymbol{M}_{42} \end{bmatrix},$$

$$\boldsymbol{M}^{qq} = \begin{bmatrix} M_{33} & \boldsymbol{M}_{34} \\ \boldsymbol{M}_{43} & \boldsymbol{M}_{44} \end{bmatrix}, \qquad \boldsymbol{N}^{p} = \begin{bmatrix} N_1 \\ N_2 \end{bmatrix}, \qquad \boldsymbol{N}^{q} = \begin{bmatrix} N_3 \\ \boldsymbol{N}_4 \end{bmatrix}, \qquad \boldsymbol{B}^{p} = \begin{bmatrix} 0 \\ 0 \end{bmatrix},$$

$$\boldsymbol{B}^{q} = \begin{bmatrix} -1 \\ 0 \end{bmatrix}, \qquad \boldsymbol{U} = [i_q^*].$$

Where the elements (e.g. $M_{11}, M_{12}, \ldots, \boldsymbol{M}_{44}, N_1, N_2, \ldots, \boldsymbol{N}_4$) are shown in [20].